Solid-State Electronics 67 (2012) 94–99

Contents lists available at SciVerse ScienceDirect

Solid-State Electronics

journal homepage: www.elsevier.com/locate/sse

Engineering the current–voltage characteristics of metal–insulator–metal diodes using double-insulator tunnel barriers

Sachit Grover *, Garret Moddel

Department of Electrical, Computer, and Energy Engineering, University of Colorado, Boulder, CO 80309-0425, United States

ARTICLE INFO

Article history:
Received 20 May 2011
Accepted 17 September 2011
Available online 10 October 2011

The review of this paper was arranged by Dr. Y. Kuk

Keywords:
MIM diode
Electron tunneling
Transfer-matrix method
MOM diode

ABSTRACT

The femtosecond-fast transport in metal–insulator–metal (MIM) tunnel diodes makes them attractive for applications such as ultra-high frequency rectenna detectors and solar cells, and mixers. These applications impose severe requirements on the diode current–voltage $I(V)$ characteristics. For example, rectennas operating at terahertz or higher frequencies require diodes to have low resistance and adequate nonlinearity. To analyze and design MIM diodes with the desired characteristics, we developed a simulator based on the transfer-matrix method, and verified its accuracy by comparing simulated $I(V)$ characteristics with those measured in MIM diodes that we fabricated by sputtering, and also with simulations based on the quantum transmitting boundary method. Single-insulator low-resistance diodes are not sufficiently nonlinear for efficient rectennas. Multi-insulator diodes can be engineered to provide both low resistance and substantial nonlinearity. The improved performance of multi-insulator diodes can result from either resonant tunneling or a step change in tunneling distance with voltage, either of which can be made to dominate by the appropriate choice of insulators and barrier thicknesses. The stability of the interfaces in the MIIM diodes is confirmed through a thermodynamic analysis.

Published by Elsevier Ltd.

1. Introduction

Metal–insulator electronics [1,2] include not just diodes [3] but a whole suite of components including varactors [4], bipolar [5] and field-effect [6] transistors, and plasmonic waveguides [7,8]. At the core of each device is a metal/insulator/metal (MIM) tunnel diode. A key application for these diodes is in the detection and mixing of radiation in millimeter wave [9] and sub-millimeter wave bands [10,11]. Active research on MIM diodes is directed towards their use in rectifying antenna-coupled diodes (rectennas) for infrared detection [7,12,13] and photovoltaic energy conversion [14–16]. These high-frequency applications require diodes with low resistance and capacitance to facilitate efficient coupling to antennas [17]. Even though MIM diodes have been around for more than five decades, their applicability in rectennas at near-infrared to visible wavelengths is still a challenge [18].

An MIM diode consists of two metal electrodes that are spaced apart by several nanometers of insulator or a stack of insulators. Conduction of charge carriers through the insulator occurs via the femtosecond-fast mechanism of quantum tunneling [19,20]. Tunneling leads to nonlinear current–voltage $I(V)$ characteristics that depend on the shape of the barrier [21]. Based on the application, a diode with a high forward-to-reverse current ratio (asymmetry) or a sharp turn-on (nonlinearity) may be required. Low-resistance single-insulator MIM diodes fail to achieve these characteristics, but they can be improved upon with the incorporation of multi-insulator barriers [3,22,23]. Hegyi et al. [24] have conducted a simulation based investigation of parameters for an optimized double-insulator (MIIM) diode. However, their implementation fails to capture the effect of resonant tunneling [3], which can significantly alter the diode behavior. In another MIIM configuration [25], an abrupt change in tunnel distance with increasing bias voltage leads to a high forward-to-reverse current ratio. We develop an in-depth understanding of these effects and use them to design experimentally-feasible MIIM diodes with improved characteristics for high frequency rectennas.

In Section 2 we describe our simulation methodology and compare the $I(V)$ characteristics of MIM diodes obtained from simulation and measurement. In Section 3, we explain the requirements for an efficient rectifier and point out the limitations of single-insulator diodes. In Section 4, we investigate the mechanisms by which double-insulators diodes can achieve better characteristics than single-insulator diodes. Based on these mechanisms, we design experimentally feasible MIIM diodes and compare their simulated characteristics with those of an MIM diode.

* Corresponding author. Present address: Silicon Materials and Devices, National Renewable Energy Laboratory, Golden, CO 80401, United States.

E-mail address: sachitgrover@ieee.org (S. Grover).

0038-1101/$ - see front matter Published by Elsevier Ltd.
doi:10.1016/j.sse.2011.09.004

2. Tunnel current simulator

2.1. Simulation methodology

The shape of the tunnel barrier is determined by the work function of the metals, the electron affinity of the insulators, and the applied voltage. In addition, an electron in the vicinity of a metal experiences an image potential that causes barrier lowering [2]. The resulting barrier shape is used to calculate the electron transmission probability which, along with the Fermi distribution of electrons in the metals, provides the tunnel current. Consider the barrier shown in Fig. 1. An electron with total energy E, has an x-directed component of energy E_x and a transmission probability $T(E_x)$. Assuming an isotropic distribution of electron velocities in the metal electrodes, the formula for the tunnel current as a function of diode voltage (V_D) is given by [26,27]

$$J(V_D) = J_{L\rightarrow R} - J_{R\rightarrow L} = \frac{4\pi m_0 e}{h^3}\int_0^{\infty} T(E_x)dE_x \int_{E_x}^{\infty}\{f_L(E) - f_R(E + eV_D)\}dE \quad (1)$$

where the Fermi–Dirac distribution functions in the left (f_L) and the right (f_R) metal electrodes are

$$f_L(E) = \frac{1}{1+\exp\left(\frac{E-E_{FL}}{kT}\right)}; \quad f_R(E+eV_D) = \frac{1}{1+\exp\left(\frac{E-(E_{FL}-eV_D)}{kT}\right)} \quad (2)$$

The transmission probability is calculated from the plane-wave solution for the Schrödinger equation obtained using the transfer-matrix method (TMM) [28] and the quantum transmitting boundary method (QTBM) [29]. Both methods give identical results, as shown in Fig. 2. In comparison, the WKB approximation gives a much higher $T(E_x)$ thereby overestimating the tunnel current. Therefore, analytical $I(V)$ formulae based on the WKB method [2,26,30] are not suitable for calculating the tunnel current in low-barrier diodes.

A more rigorous simulation technique is the Green's function method [31], which is computationally intensive. We use the TMM for its ease of implementation. Also, the TMM uses a conduction band approximation to calculate the barrier for tunneling, which provides a visual aid for the design of tunnel diodes. In implementing the TMM we ensure its numerical stability and avoid round-off errors by combining the wavefunction boundary conditions for all the discrete element given by individual 2 × 2 matrices into a combined block-diagonal matrix [32].

We assume a perfect insulator for a solely tunneling-based analysis of the $I(V)$ characteristics. In an experimental diode, conduction through defects, surface states, and charge build-up at the interfaces can affect the current. Thicker diodes with bulk-limited conduction [27] may have non-tunneling electron transport mechanisms that contribute to the total current, but for the thin diodes of interest the pure tunneling analysis provides accurate simulations, as verified below.

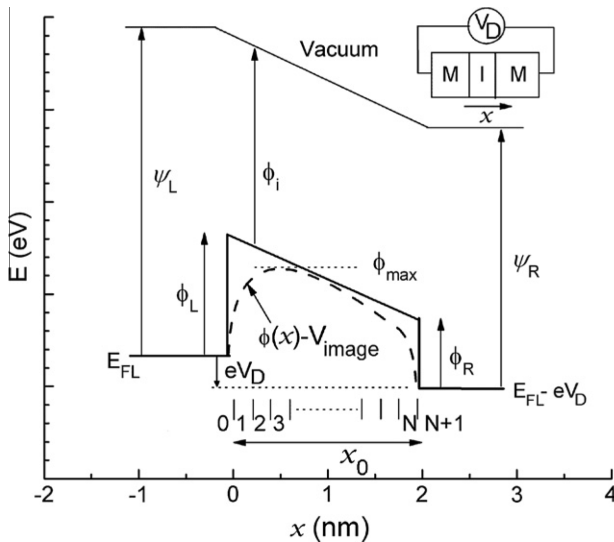

Fig. 1. Energy-band diagram for an asymmetric ($\phi_L \neq \phi_R$) tunnel barrier. Here, φ_i is the electron affinity of the insulator, ψ is the metal work function, and V_D is the voltage applied across the diode. The Fermi level of the left metal electrode (E_{FL}) is held fixed while that of the right electrode varies with the applied voltage. The rectangular barrier is modified by the image-force barrier lowering to give the effective barrier profile (dashed).

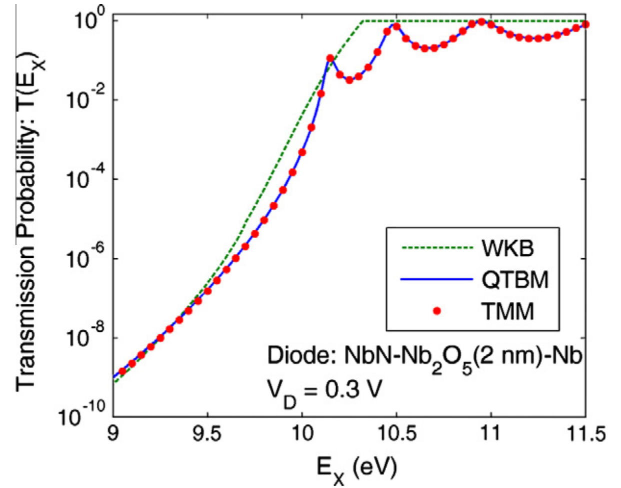

Fig. 2. Log-scale plot of the transmission probability $T(E_x)$ vs. the x-directed energy of the electron (E_x) obtained from the transfer matrix (TMM) (solid), the WKB (dashes), and the quantum transmitting boundary (QTBM) (dots) methods. The TMM and the QTBM give identical values for $T(E_x)$, while the WKB approximation overestimates the transmission probability.

2.2. Comparison with experiment

Simulated and experimental characteristics of two asymmetric MIM diodes are compared in Fig. 3. The diodes are made from sputtered insulator and metal layers and the dimensions shown are the targeted thickness of the insulators based on the deposition conditions and time. The parameters for the materials, used in

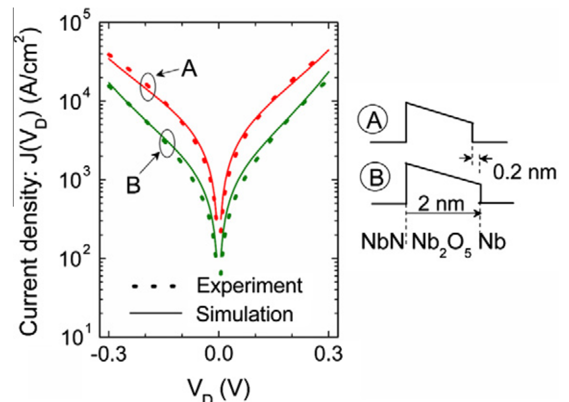

Fig. 3. Comparison of simulated and experimental $I(V)$ characteristics for two MIM diodes. The simulated curves obtained from the transfer matrix method are in close agreement with experimental characteristics. The insulator widths used in the diode simulations are as targeted during deposition.

Table 1
Material parameters for metals and insulators used in the simulations.

Metal	Work function (eV)	Insulator	Electron affinity (eV)	Dielectric constant
Nb [40]	4.33	Nb_2O_5 [40]	4.23	25
NbN [40]	4.7	Ta_2O_5 [40]	3.83	20
W [41]	4.55			

the simulation, are given in Table 1. The simulated $I(V)$ curves are in good agreement with the measured characteristics.

In the absence of an experimental estimate, the effective mass of the electron in the insulator (m_e) is assumed to be equal to the rest mass (m_0) [33]. Unlike crystalline semiconductors, for which m_e can be obtained from the band structure [34], the amorphous insulators under consideration require a direct experimental measurement to determine the effective mass [35].

2.3. Simulating multi-insulator diodes

In a multi-insulator diode, the dielectric constants of the insulators play an important role in determining the voltage drop across each insulator layer. To determine the energy-band profile at a certain bias (V_{bias}), we apply the condition for continuity of the electric displacement vector at each insulator interface and obtain the voltage drop across each layer

$$\Delta V_j = (V_{bias} - V_{bi})\frac{x_j/\varepsilon_j}{\sum x_j/\varepsilon_j} \tag{3}$$

where x_j and ε_j represent the thickness and dielectric constant, respectively, of the jth layer, and $V_{bi}(=\psi_L-\psi_R)$ is the built-in potential.

In a multi-insulator diode, the effect of the image force is calculated as

$$V_{image}(x) = -\frac{e^2}{16\pi\varepsilon_0}\left(\frac{1}{\int_0^x \varepsilon(x')dx'} + \frac{1}{\int_x^L \varepsilon(x')dx'}\right) \tag{4}$$

where $L = \sum_1^K x_j$ with K being the number of insulator layers. The integrals in the denominator represent the effective distance of an electron from the left or the right metal electrode, while accounting for the changing dielectric constant.

3. Shortcomings of single-insulator (MIM) diode

Eliasson [3] has extensively analyzed the possible variations of a single-insulator MIM diode. In a rectenna, a low resistance diode is necessary for efficient coupling to the antenna [18], and is achieved by keeping the barrier heights low. A high responsivity is required for efficient square-law (small-signal) rectification [17]. The responsivity is a measure of the diode nonlinearity and is defined at the operating voltage of interest as $\beta = I''/(2I')$ [17]. It is the DC current generated in the diode per unit of incident AC power. The $I(V)$ characteristics of the diode depend on the shape of the tunnel barrier, which is determined by the metals and insulators used to form the diode. To optimize the diode resistance and responsivity, the variable parameters are the barrier heights φ_L, φ_R and the insulator thickness.

Here we analyze these characteristics of several diodes. To make the comparison of multiple diode having different variation of resistance and responsivity with voltage tractable, we carry out the analysis at zero bias. In the comparison of MIM and MIIM diodes given in the next section it will become evident that MIIM diodes are superior even at a non-zero bias. At zero bias, the responsivity is determined by the degree of asymmetry in the tunnel barrier heights, which results in the asymmetry in the $I(V)$ curves. In Fig. 4a and b, we plot the responsivity and resistance vs. the difference in barrier height on the left (φ_L) and the right

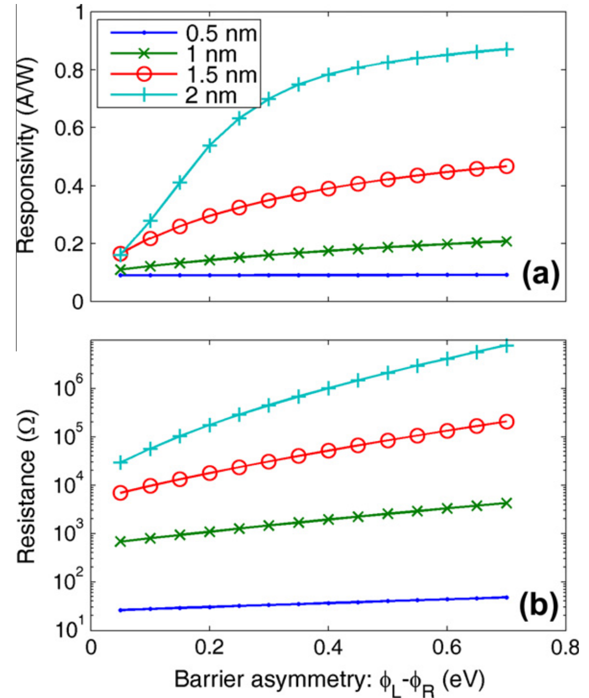

Fig. 4. (a) Responsivity and (b) resistance vs. barrier asymmetry for single-insulator diodes at zero bias. The diode thickness and the left barrier height (φ_L) are varied while the right barrier height (φ_L) is kept fixed at 0.1 eV. The responsivity increases with increase in asymmetry but saturates for high $\varphi_L - \varphi_R$. For the same asymmetry, the responsivity is larger for thicker diodes. Increasing asymmetry and increasing thickness both lead to larger resistance.

(φ_R). Experimentally, this can be achieved by changing the metal on the left while keeping the insulator and the metal on the right fixed. As seen in Fig. 4a, only a small improvement in responsivity is obtained by increasing the barrier asymmetry for thin barriers but a substantial change for thicker barriers. However, the responsivity saturates at large asymmetry. For a fixed asymmetry, the responsivity is higher for thicker barriers, as shown in Fig. 4b. As the responsivity increases with increasing asymmetry or increasing thickness, so does the resistance. In a rectenna, this negates the improvement in responsivity as the impedance match between the antenna and the diode becomes worse [18].

4. Double-insulator (MIIM) configurations

To obtain a high responsivity and low resistance diode, one can design an MIIM barrier with resonant tunneling [3,36]. Alternatively, an MIIM configuration can be designed to have a step-change in tunneling distance with voltage [25]. Both these mechanisms can occur in the same diode, with the overall asymmetry of the $I(V)$ curve regulated by the one that dominates. We examine these effects through the simulation of two double-insulator tunnel diodes.

Consider two MIIM diodes that have the same materials but different insulator thicknesses. Diode MIIM1 consists of W–Nb_2O_5 (3 nm)–Ta_2O_5(1 nm)–W, and MIIM2 consists of W–Nb_2O_5(1 nm)–Ta_2O_5(1 nm)–W. The material parameters are listed in Table 1. This

choice of materials and dimensions is not optimized for maximum nonlinearity or current but rather is chosen to demonstrate the difference between the resonant tunneling dominant in MIIM1 and the step change dominant in MIIM2.

For the two diodes, the conduction band profiles under positive and negative bias are shown in Fig. 5. A quantum well is formed in both MIIM diodes under positive bias (a) and (b). However, only in the MIIM1 is the quantum well wide enough to have a resonant energy level. On the other hand, under negative bias (c) and (d), only the step barrier-profile in MIIM2 leads to an abrupt change in the tunneling distance for the electrons near the Fermi level on the right metal-electrode.

The transmission probability for the four barrier profiles of Fig. 5 is shown in Fig. 6. The Fermi level at the left metal electrode is fixed at 10 eV. For low electron energies, the transmission probability $T(E_x)$ for the step (MIIM2) diode, represented by curves (b) and (d), is higher than for the resonant (MIIM1) diode, represented by (a) and (c). With increasing E_x, the transmission probability for the resonant diode at positive bias rises sharply near the resonant tunneling peak. Despite the barrier's larger thickness, the resonance peak rises higher than (b). The negative bias transmission probability in the resonant diode, (c), remains lower than in the step diode, (d), for most of the energy range that contributes to the net electron current ($10 < E_x < 10.4$ eV). As E_x rises above the highest potential on the low-barrier insulator, the transmission probability exhibits oscillatory behavior for all four cases. In this energy range, the electrons tunnel through the high-barrier while the interference of the wavefunction in the low-barrier causes oscillations. These oscillations modify the probability of tunneling through the higher barrier to give the net transmission probability.

The $I(V)$ characteristics for the resonant and step diodes are shown in Fig. 7a. In the step diode, the tunneling distance for an electron under negative bias is small and hence the direct tunneling gives a large current. For the resonant diode, the resonant tunneling results in a larger current under positive bias, where the Fermi level for the metal at the left approximately matches

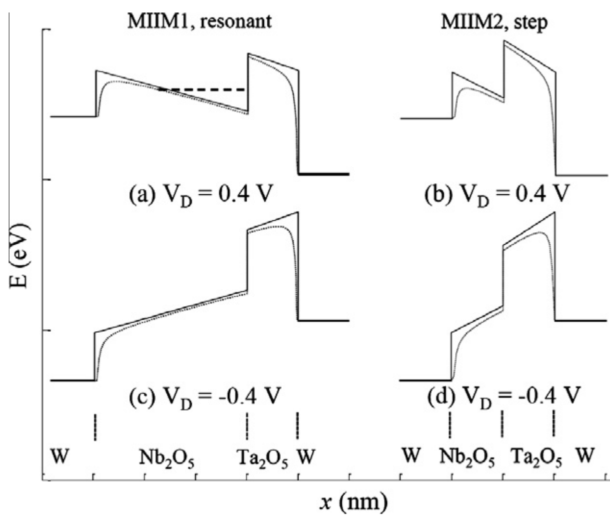

Fig. 5. Energy-band profiles for the resonant and step MIIM diodes. Forward and reverse bias profiles are shown respectively in (a) and (c) for the resonant, and in (b) and (d) for the step diode. The dotted lines show the profiles with barrier lowering. The diode parameters are given in Table 1. The thickness of the Nb_2O_5 layer is the only difference between the two diodes.

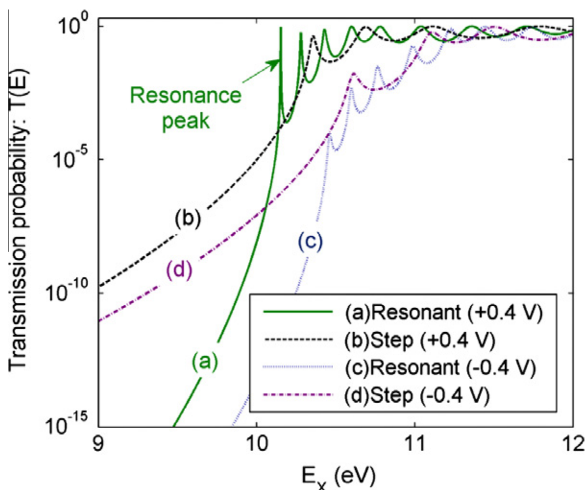

Fig. 6. Electron transmission probabilities for the resonant and step MIIM diodes of Fig. 5. The diode parameters are given in Table 1. A sharp resonance peak is observed in the resonant diode under forward bias due to the formation of a quantum well.

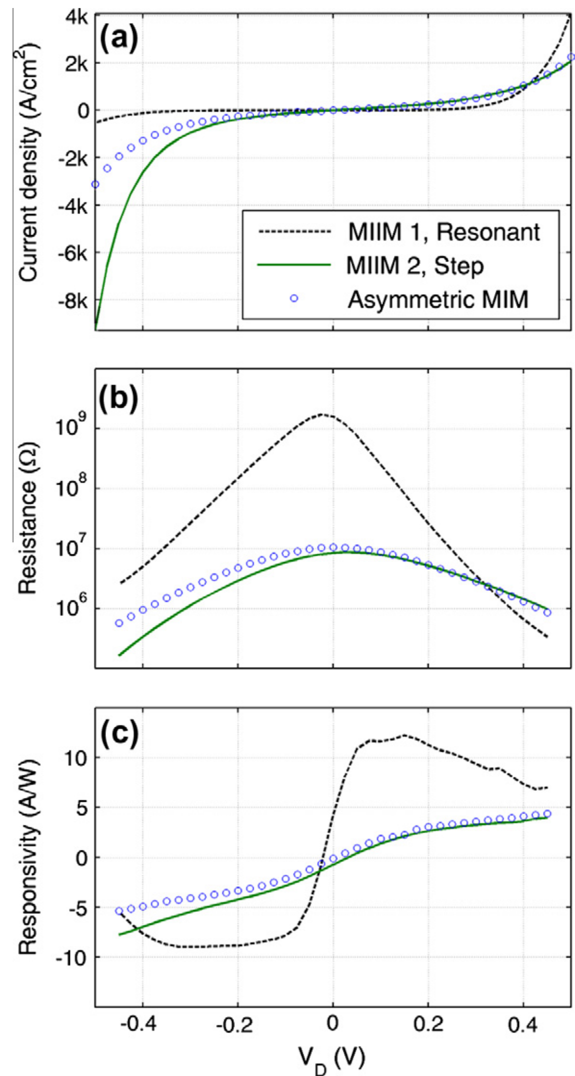

Fig. 7. (a) Current density vs. voltage for the MIIM diodes shown in Fig. 5, and a comparable asymmetric-MIM diode. The step MIIM diode has higher current magnitude under negative bias due to the direct tunneling of electrons across the high-barrier. The resonant MIIM diode has the opposite asymmetry in its $I(V)$ characteristic, due to the formation of resonant quantum well under positive bias. Comparing these with an asymmetric MIM diode we see that both the MIIM diodes have a smaller resistance (b) and larger nonlinearity (c) in their preferred direction of conduction.

the energy of the resonant well, than the direct tunneling under negative bias. Thus a sharper rise in current is seen under negative bias in the step diode and under positive bias in the resonant diode.

In Fig. 7a, we also compare the MIIM diodes to an asymmetric-MIM diode with barrier heights corresponding to a W–Nb_2O_5 interface on the left and a Ta_2O_5–W interface on the right and an insulator thickness of 2 nm. The asymmetric-MIM diode is effectively the MIIM2 diode without the abrupt step in the conduction band profile. This is confirmed by their similar current densities under positive bias. However, under negative bias the step change in tunnel distance in MIIM2 causes a sharp increase in tunnel current. This difference is also evident in the resistance and responsivity curves in Fig. 7b and c where, under negative bias, the sharp increase in current for MIIM2 leads to a lower resistance and a higher responsivity. The resistance of the resonant diode is significantly higher at zero bias but becomes comparable to the thinner diodes near V_D = 0.4 V. The large change in resistance corresponds to the higher magnitude of responsivity. Thus, the mechanisms that increase the nonlinearity result in MIIM diodes with higher responsivity and lower differential resistance than an equivalent MIM diode of comparable current density.

The above example shows that just changing the thickness of an insulator in an MIIM diode can lead to different asymmetry and nonlinearity. It does not suggest which of the mechanisms for achieving larger nonlinearity is preferable. We have analyzed several MIIM diodes designed for implementing these mechanisms and the performance improvement over MIM diodes is observed consistently. The mechanisms exemplified in MIIM diodes can also be applied to barriers with more than two insulators [37].

5. Thermodynamic stability

Sub-micron scale lithography and advanced deposition techniques have enabled the fabrication of metal–insulator diodes with a variety of materials and precise control over layer thicknesses. However, an arbitrary combination of metals and insulators may not be stable. A thermodynamic analysis of the interface stability is required to determine whether the intended barriers may be obtained in an experimental device. For the MIIM diodes discussed in the previous section, we have carried out a Gibb's free energy analysis [38] for reaction between all interfacial pairs of materials using the FACTsage web software [39]. We analyze each of the pairs at room temperature and at 1000 K and confirm that no unintended interfacial compounds are formed.

6. Conclusions

We analyze the current–voltage characteristics of single -insulator MIM diodes and two double-insulator configurations. A comparison of thick and thin double-insulator diodes shows that the bias direction causing higher current depends on the electron-transmission-limiting mechanism. If a resonant energy-level is achievable under a particular bias, the current for this polarity can become larger than that under the opposite bias. In the absence of a resonant level, the step change in tunneling distance under the opposite bias causes the larger current. Compared to single-insulator diodes, both the resonance and the step-change mechanisms in double-insulator diodes result in a larger responsivity and a smaller resistance.

Acknowledgments

We thank Olga Dmitriyeva, Xi Chen, and David Doroski for helping with the fabrication and measurement of the MIM diodes. This work was partially supported by DARPA through US Army Aviation & Missile Command Contract No. W31P4Q-06-C-0296. We gratefully acknowledge additional partial support through a contract from Abengoa Solar.

References

[1] Michael Kale B. Electron tunneling devices in optics. Opt Eng 1985;24(2):267–74.
[2] Sze SM, Ng KK. Physics of semiconductor devices. 3rd ed. Wiley-Interscience; 2006.
[3] Eliasson BJ. Metal–insulator–metal diodes for solar energy conversion. University of Colorado at Boulder, Boulder. PhD Thesis; 2001..
[4] Estes MJ. Metal–insulator varactor devices. US patent No. 7388,276, June 17, 2008.
[5] Estes MJ, Eliasson BJ. Thin-film transistors based on tunneling structures and applications. US patent No. 7173,275; 2006.
[6] Fujimaru K, Matsumura H. Theoretical consideration of a new nanometer transistor using metal/insulator tunnel-junction. Jpn J Appl Phys 1996;35:2090–4.
[7] Grover S, Dmitriyeva O, Estes MJ, Moddel G. Traveling-wave metal/insulator/metal diodes for improved infrared bandwidth and efficiency of antenna-coupled rectifiers. Nanotechnol IEEE Trans 2010;9(6):716–22.
[8] Estes Michael J, Garret Moddel. Surface plasmon devices. US patent No. 7010,183; 2006.
[9] Rockwell S et al. Characterization and modeling of metal/double-insulator/metal diodes for millimeter wave wireless receiver applications. In: Radio Frequency Integrated Circuits (RFIC) Symposium IEEE, 2007. p. 171–4.
[10] Fumeaux C, Herrmann W, Kneubühl FK, Rothuizen H. Nanometer thin-film Ni–NiO–Ni diodes for detection and mixing of 30 THz radiation. Infrared Phys Technol 1998;39(3):123–83.
[11] Abdel-Rahman MR, Gonzalez FJ, Zummo G, Middleton CF, Boreman GD. Antenna-coupled MOM diodes for dual-band detection in MMW and LWIR. Proc. SPIE 2004;5410:233–8.
[12] Sarehraz M. Novel rectenna for collection of infrared and visible radiation. University of South Florida, PhD Thesis. 2005.
[13] Hobbs Philip C, Laibowitz Robert B, Libsch Frank R, LaBianca Nancy C, Chiniwalla Punit P. Efficient waveguide-integrated tunnel junction detectors at 1.6 μm. Opt Express 2007;15(25):16376–89.
[14] Mario Dagenais, Kwangsik Choi, Filiz Yesilkoy, Chryssis Athanasios N, Peckerar Martin C. Solar spectrum rectification using nano-antennas and tunneling diodes. Proc. SPIE 2010;7605:76050E.
[15] Bhansali S, Krishnan S, Stefanakos E, Goswami DY. Tunnel junction based rectenna—a key to ultrahigh efficiency solar/thermal energy conversion. AIP Conf Proc 2010;1313(1):79–83.
[16] Osagie Imafidon, Stavros Georgakopoulos, Phani Kiran Vabbina, Nezih Pala. Multifunctional nanodevices for energy harvesting in unconventional spectral ranges. Proc. SPIE 2010;7679:76792L.
[17] Sanchez Jr A, Davis CF, Liu KC, Javan A. The MOM tunneling diode: theoretical estimate of its performance at microwave and infrared frequencies. J Appl Phys 1978;49(10):5270–7.
[18] Grover S, Moddel G. Applicability of metal/insulator/metal (MIM) diodes to solar rectennas. IEEE J. of Photovoltaics, in press.
[19] Hartman Thomas E. Tunneling of a wave packet. J Appl Phys 1962;33(12):3427–33.
[20] Moichiro Nagae. Response time of metal–insulator–metal tunnel junctions. Jpn J Appl Phys 1972;11(11):1611–21.
[21] Stratton R. Volt–current characteristics for tunneling through insulating films. J Phys Chem Solids 1962;23(9):1177–90.
[22] Likharev KK. Layered tunnel barriers for nonvolatile memory devices. Appl Phys Lett 1998;73(15):2137–9.
[23] Casperson JD, Bell LD, Atwater HA. Material issues for layered tunnel barrier structures. J Appl Phys 2002;91(1):261–7.
[24] Hegyi B, Csurgay A, Porod W. Investigation of the nonlinearity properties of the DC *I–V* characteristics of metal–insulator–metal (MIM) tunnel diodes with double-layer insulators. J Comput Electron 2007;6:159–62 [10.1007/s10825-006-0083-9].
[25] Yoshinari Matsumoto, Tatsuro Hanajiri, Tohru Toyabe, Takuo Sugano. Single electron device with asymmetric tunnel barriers. Jpn J Appl Phys 1996;35:1126–31.
[26] Simmons John G. Generalized formula for the electric tunnel effect between similar electrodes separated by a thin insulating film. J Appl Phys 1963;34(6):1793–803.
[27] Simmons JG. Conduction in thin dielectric films. J Phys D Appl Phys 1971;4(5):613.
[28] Ghatak AK, Thyagarajan K, Shenoy MR. A novel numerical technique for solving the one-dimensional Schroedinger equation using matrix approach-application to quantum well structures. IEEE J Quant Electron 1988;24(8):1524–31.
[29] Lent Craig S, Kirkner David J. The quantum transmitting boundary method. J Appl Phys 1990;67(10):6353–9.
[30] Chapline Michael G, Wang Shan X. Analytical formula for the tunneling current versus voltage for multilayer barrier structures. J Appl Phys 2007;101(8):083706.
[31] Datta S. Quantum transport: atom to transistor. Cambridge; 2005.

[32] Probst Oliver M. Tunneling through arbitrary potential barriers and the apparent barrier height. Am J Phys 2002;70(11):1110–6.
[33] Grossman EN, Harvey TE, Reintsema CD. Controlled barrier modification in Nb/NbOx/Ag metal insulator metal tunnel diodes. J Appl Phys 2002;91(12):10135–9.
[34] Kittel C. Introduction to solid state physics. 7th ed. John Wiley & Sons; 1996. p. 209.
[35] Solymar L, Walsh D. Electrical properties of materials. 8th ed. Oxford University Press; 2010. p. 143.
[36] Moddel G, Eliasson BJ. High speed electron tunneling device and applications. US patent No. 6756,649; 2004.
[37] Korotkov A, Likharev K. Resonant Fowler-Nordheim tunneling through layered tunnel barriers and its possible applications. Techn Dig IEDM 1999:223–6.
[38] Silberberg MS. Principles of general chemistry. New York: McGraw-Hill; 2007. p. 666.
[39] Bale CW. FACT-EQUILIB-Web. February 2011. <http://www.crct.polymtl.ca/equiwebmenu.php>.
[40] Phiar Corporation. Private communication. 2007.
[41] Camp M, Lecchini SMA. The work function of polycrystalline tungsten foil. Proc Phys Soc 1965;85(4):815.